Testing for Welding, Joining or Additive Manufacturing Applications

Tanju Teker* and Denizer Gençdoğan

Mechanical performance and weldability of HARDOX 450/AISI 430 grade joined by TIG double-sided arc welding

https://doi.org/10.1515/mt-2022-0090

Abstract: AISI 430 and HARDOX 450 grades were combined using tungsten inert gas double-sided welding process. Microstructural changes were evaluated with scanning electron microscope, energy dispersive spectrometry, electron back scatter diffraction, elemental mapping, X-ray diffraction analysis. Mechanical diffenrences of welded alloys were determined by tensile, notch impact and microhardness tests. Failure surfaces of tensile samples were examined by SEM. The maximum tensile strength was 513.59 MPa and the impact energy was 77 J at welding speed of 0.01 m min^{-1} at current of 475 A. The lowest hardness was determined in HAZ due to excessive grain size. Failure exhibited brittle fracture and cleavage planes.

Keywords: AISI 430; DSAW; HARDOX 450; mechanical performance; microstructure.

1 Introduction

Tungsten inert gas (TIG) welding is a high efficiency, quality, sensitive and clean technique. TIG process is preferred in different industry operations. TIG welding parameters are the most prominent variables affecting the grade, performance and expenditure of the joint [1–3]. The size and form of the weld bead is important to welding engineers in the manufacturing industry. Bead geometry clearly affects the construction and fabrication costs of steel structures and mechanical tools. Welding of different metals has attracted attention because it reduces costs and saves materials [4–6]. Ferritic stainless steels (FSS) are iron–chromium alloys with a body-centered cubic (BCC) crystal structure. They have a quite weaker strength, ductility and formability at higher temperatures than the austenitic type. FSS is preferred in the chemical processing industry, furnace parts, petroleum refining equipment, protection tubes, storage containers, electrical appliances. Ferritic alloys are difficult to join due to the number of brittle precipitates and metallurgical changes. Different problems can be encountered in the welding of ferritic stainless steels. Grain size is a serious problem in the welding of FSSs and coarse grains lead to lower toughness. FSS is a good alternative to austenitic stainless steel, particularly for practices needing nickel-free stainless steel [7–11]. HARDOX grade is classified according to its kinds, thick, carbon rate and alloy elements (Ni, Mn, Cr, Mo, B). HARDOX steel is produced in 400, 450, 500, 550 and 600 type. HARDOX-450 has ideal abrasion resistance, combinability, cold bending and hardness [12]. Cheng et al. [13] reported the butt joinability of titanium and stainless steel with Cu insert wire using double-sided MIG-TIG welding. The strength of the butt joint was achieved as 278 MPa. Ti-Fe intermetallic compounds formed in the structure with low heat input and rapid cooling in the arc welding were removed from the structure.

In this study, AISI 430 and HARDOX 450 steels were combined using the TIG double-sided arc welding. Mechanical characteristics and weldability of joints were analyzed.

2 Experimental approach

HARDOX 450 and AISI 430 ferritic stainless steels in dimensions of $125 \times 100 \times 10$ mm^3 as the sheet alloy were used. The chemical composition of steels used in tests is given in Table 1. The mechanical values of the test materials are provided in Table 2. Welding production parameters for welded joints are presented in Table 3. Ge-Ka-Mak welding machine was used for joints. Extraction of test samples from welded joints is given in Figure 1. Samples were flatted using 180–1200 mesh SiC sanding papers and polished using diamond paste. HARDOX 450 side was etched by immersion

***Corresponding author: Tanju Teker**, Department of Manufacturing Engineering, Faculty of Technology, Sivas Cumhuriyet University, 58140, Sivas, Turkey, E-mail: tanjuteker@cumhuriyet.edu.tr
Denizer Gençdoğan, Pazarcık Aksu Vocational and Technical Anatolian School, Kahramanmaraş, Turkey

in nital solution. AISI 430 side was electrolytically etched with Vilella's reagent of 1 g picric acid, 5 mL HCl acid, 100 mL ethyl alcohol at a voltage of 5 V in 10 s. The microstructural changes occurring in welded joints were determined using a ZEISS EVO LS10 scanning electron microscope (SEM), energy dispersion spectrometry (EDS), electron back scatter diffraction (EBSD), elemental mapping, a Bruker X-ray diffraction (XRD). The quality and mechanical properties of the welds were evaluated by tensile test, notch impact and hardness tests. Tensile test was applied to the samples prepared according to ASTM E8M–04 standard with 100 kN Instron test system [14]. Charpy impact test was applied to samples prepared according to ASTM E23-06 standard at room temperature [15]. The dimensions of tensile and charpy test samples are shown in Figures 2 and 3. Fracture morphology of the tensile test specimens was observed by using SEM.

3 Experimental results

3.1 Macro and microstructure

Macro structure images of double-sided TIG welded joints are shown in Figure 4. Weld seams did not show any physical faults. In the cross-sectional area of S1-S2 samples, unjoined zone was formed. Full penetration and hourglass style occurred with the increased current density in S3 sample.

SEM micrographs obtained from the welded joints are shown in Figure 5. No cracks were detected in the microstructures of the joints. As seen in SEM microstructure photographs, grain growth occurred on the AISI 430 side due to increased current intensity and increased cooling rate. Grain border, lath type and peppery carbides were formed in the microstructure [16]. Dendritic and columnar grain structure appeared in the weld area. The grain boundary martensites and carbides scattered in the grains are displayed in Figure 5. On the HAZ-HARDOX 450 side, the area under the influence of a wider heat occurred. In this zone, lath-shape martensite, acicular and widmanstatten

Table 1: Chemical composition of steels used in tests (wt%).

	Chemical composition					
Materials	**Fe**	**C**	**Cr**	**Ni**	**Si**	**Mn**
AISI 430	Bal.	0.048	16.02	0.22	0.44	0.61
HARDOX 450	Bal.	0.19	0.25	0.025	0.70	1.60

Table 2: Mechanical values of AISI 430 and HARDOX 450 steels.

Materials	Tensile strength (MPa)	Impact strength (J)	Hardness (HB)
AISI 430	485	28	182
HARDOX 450	1380	50	425–475

Table 3: Production parameters for double-sided TIG weld joining.

Sample no	Current amper (A)	Gas flow rate (l min^{-1})	Welding speed (m min^{-1})
S1	445	15	0.01
S2	460	15	0.01
S3	475	15	0.01

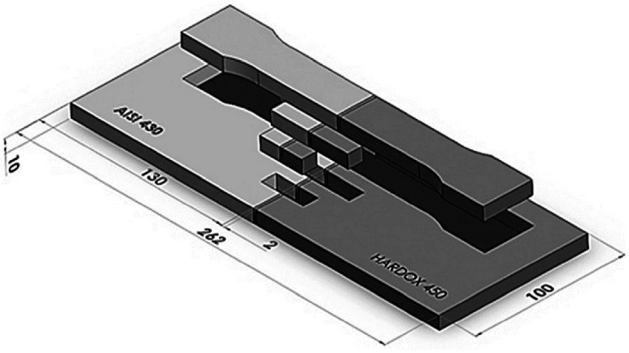

Figure 1: Extraction of test samples from welded joints.

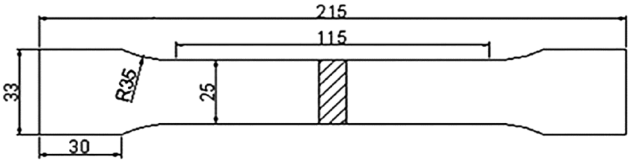

Figure 2: The measurements of the tensile test specimens.

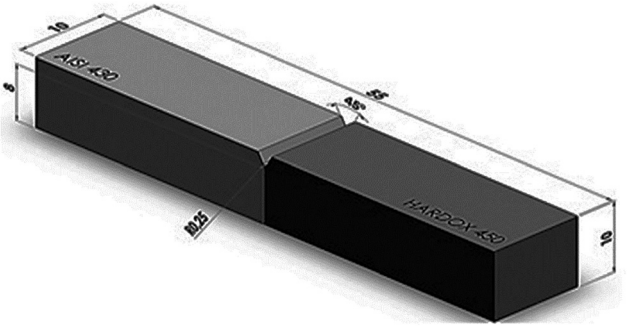

Figure 3: Scheme of the notch impact test sample.

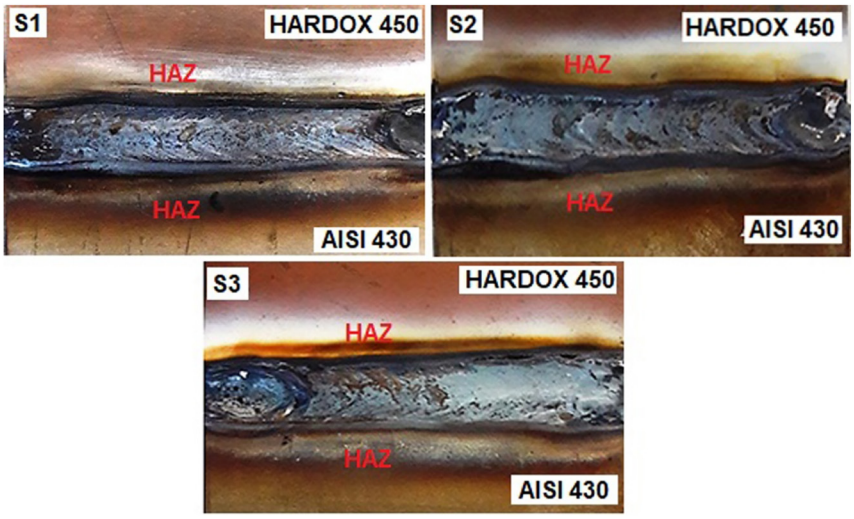

Figure 4: Surface and cross-sectional macrostructure images of test samples.

ferrite were observed depending on the cooling and the carbon rate. XRD analysis of S3 sample are dedicated in Figure 6. Fe, Cr_7C_3, Cr_3Ni_3, $Cr_{1.36}Fe_{0.52}$ phases and compounds were detected. Welding metal electron backscatter diffraction analysis of S3 sample is given in Figure 7. The concentration compound was determined as 92% Cr_7C_3, 4% nmartensite and 4% $Cr_{23}C_6$.

EDS point analyzes of S3 sample are indicated in Figure 8. The atomic weights of different elements are exhibited in Table 4. Weld alloy and parent metal included Fe, Cr, Mn, Ni, Mo, C and Si elements. The fusion zone was enhanced with Fe, Cr, Ni and Mo, and fine dispersed precipitates detected. In metals containing

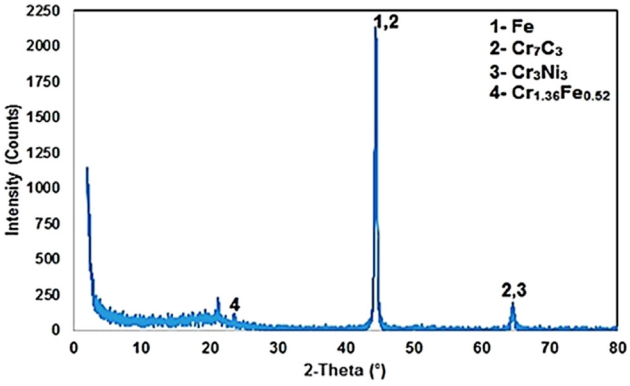

Figure 6: XRD analysis of S3 sample.

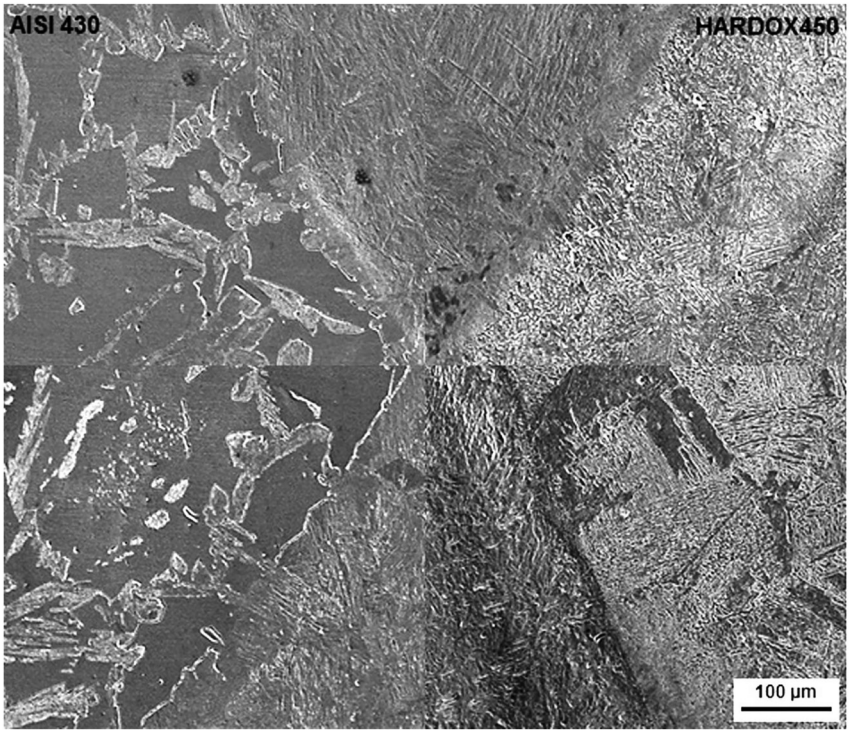

Figure 5: SEM micrographs of S3 sample.

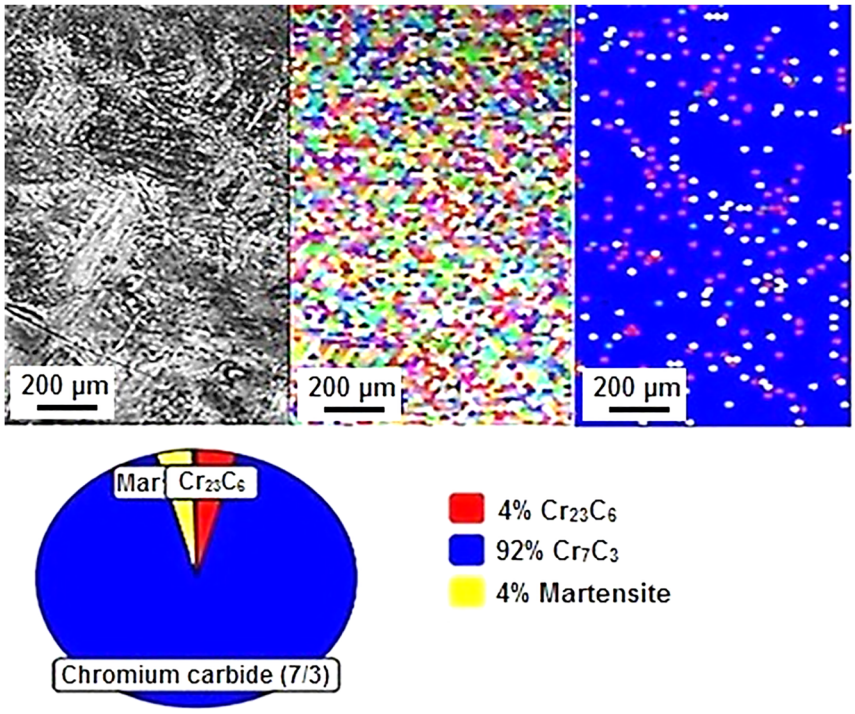

Figure 7: EBSD analysis of S3 sample.

element in unlike proportions, diffusion raised with increasing current intensity. A transition element carbon more easily dispersed into stainless steel. The diffusion of chromium and carbon elements increased with the heat density of the high current.

3.2 Microhardness

The upside and underside microhardness values of the test samples are demonstrated in Figure 9. The highest hardness was seen in the weld metal, the lowest hardness was

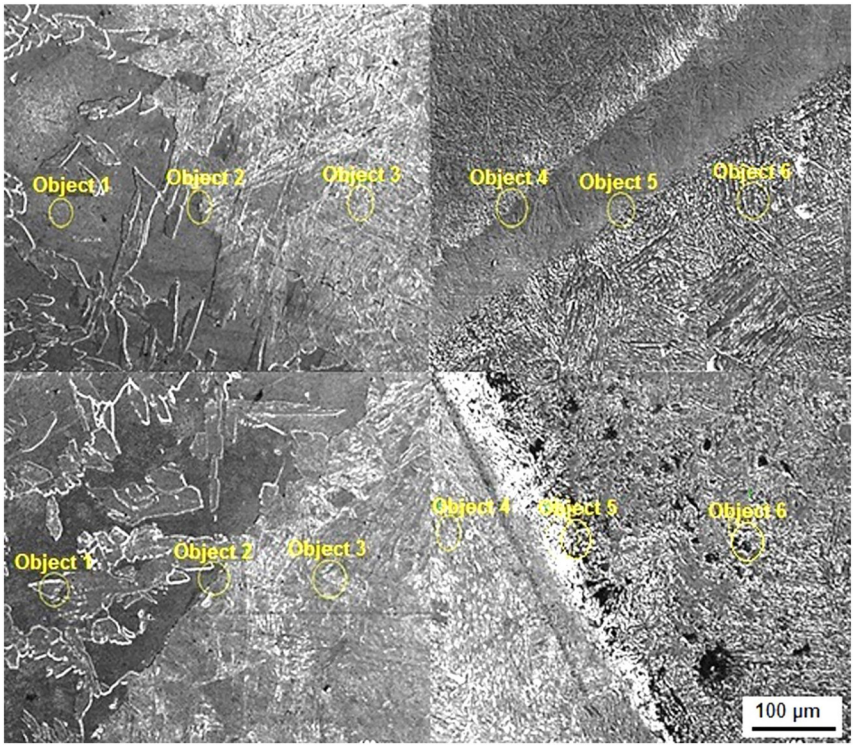

Figure 8: EDS point analyzes of S3 sample.

Table 4: EDS analysis of S3 sample.

Sample no.		Analysis objects	Elements (wt%)						
			Fe	Cr	Mn	Mo	Ni	C	Si
S3	Upside	1. Object	71.00	16.18	6.81	0.56	1.01	3.62	0.82
		2. Object	72.62	13.80	7.52	0.64	0.86	3.74	0.82
		3. Object	73.80	10.66	7.41	0.58	0.86	6.13	0.56
		4. Object	77.91	3.55	8.03	0.61	0.77	8.61	0.52
		5. Object	74.48	0.62	7.76	0.52	0.69	15.49	0.44
		6. Object	69.43	9.55	7.38	0.58	0.95	11.64	0.47
	Underside	1. Object	71.24	15.65	7.19	0.65	0.89	3.70	0.67
		2. Object	72.13	14.48	7.02	0.49	0.90	4.14	0.84
		3. Object	73.79	11.58	7.62	0.64	1.01	4.53	0.82
		4. Object	56.76	0.68	5.79	0.31	0.63	35.64	0.19
		5. Object	75.18	0.53	7.47	0.47	0.51	15.47	0.38
		6. Object	71.89	7.34	7.48	0.48	0.86	11.41	0.56

in the HAZ. The highest values were seen as upside seam S3 = 374 HV and underside seam S3 = 370 HV. The hardness measurement had almost similar values. The formation of martensite in the weld metal and the condensation of chromium carbides in the weld metal increased the hardness. The hardness of HAZ was higher than that of AISI 430 parent steel. At the weld metal melting limit, hardness was first decreased and then increased. This occurred by the diffusion of carbon into the weld metal by HARDOX 450 and chromium into the weld metal by AISI 430 due to high heat input [17]. Since martensite appeared in the HAZ of AISI 430, its hardness was higher than that of the AISI 430 master alloy. The increased hardness of HAZ was the result of grain inner and grain boundary martensite and carbide formation. The increased hardness in the weld provided strength in the joint, but reduced the toughness [18, 19]. There were two reasons for this: martensite at ferrite grain boundaries and intragranular carbide deposits. On the HAZ side of AISI 430 steel, the hardness dropped abruptly near the fusion line.

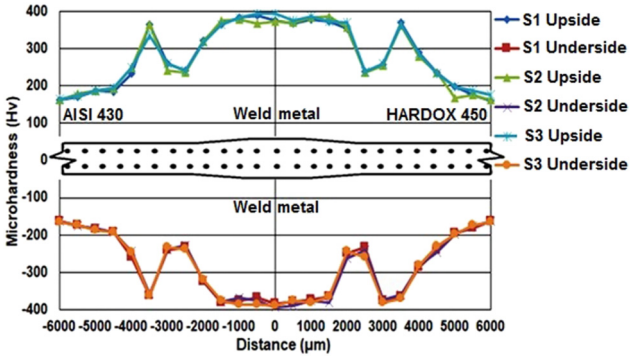

Figure 9: Upside-underside microhardness plots of test samples.

3.3 Notch impact test

Absorbed impact energies of AISI 430 and HARDOX 450 welded joints were obtained as S1 = 54 J, S2 = 68 J, S3 = 7 J. Macro photographs of notch impact test samples are given in Figure 10, and the graph of the impact results are given in Figure 11. There was a linear increase in impact resistance with increasing current intensity at joints. The most absorbed impact energy was achieved as S3 = 77 J. In the combinations made at low current intensity, the gaps formed due to the lack of full penetration created a notch effect. Low impact energies were measured at the joints at low current intensities. The fractures in the samples occurred in the zone between the AISI 430 material and the weld metal. These fractures were caused by grain size, chromium carbide precipitation and martensite [16].

3.4 Tensile test

Macro images of the S1–S3 samples after the tensile test are given in Figure 12. Tensile strength values were obtained as S1 = 383.04, S2 = 412.71 and S3 = 513.59 MPa. It was determined

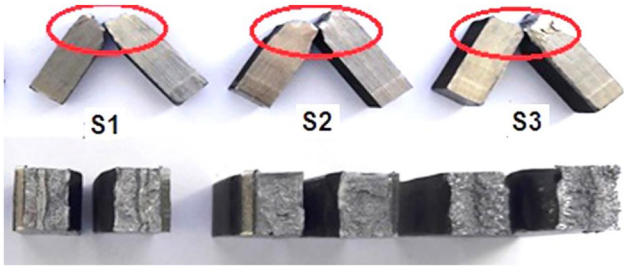

Figure 10: Impact test fracture samples.

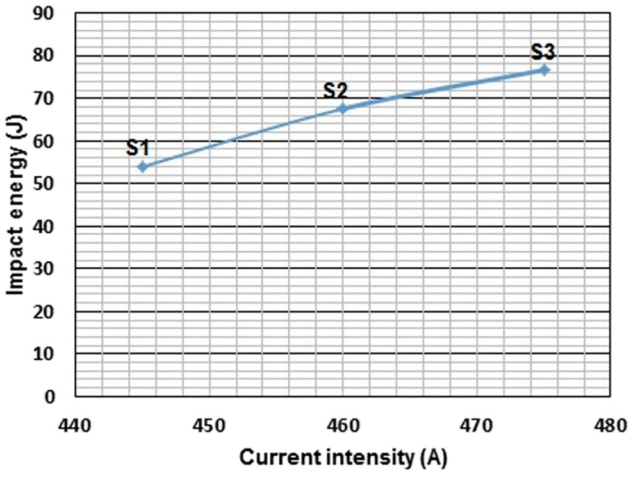

Figure 11: Graph of impact energies of S1–S3 samples.

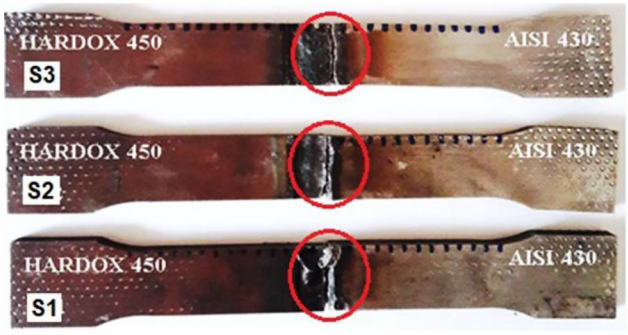

Figure 12: Macro view of tensile test specimens.

that there was a rupture on the side of AISI 430 material and very little plastic deformation occurred. This situation occurred due to chromium carbide precipitation, martensite formation and a brittle structure depending on grain size in AISI 430-HAZ [20, 21]. The chemical composition of the weld alloy changed with respect to the parent metal and the ductility of the structure in the molten zone decreased. The reason for this was the presence of duplex microstructure of martensite and ferrite. Dissimilar grain shape lead to distinct flexibility modules. The tension intensified at the boundary and a crack appeared. Long grains had lower toughness and tended to crack under cyclic loading status. In addition, martensites and carbides in grain boundaries increased hardness. This contributed to the reduction of ductility and toughness. The creation of martensite during the weld thermal cycle could be determined by the Kaltenhauser Ferrite Factor (KFF) [22]. KFF was calculated as 14.70<17. Martensite was anticipated in the weld metal of the joint.

3.5 Fracture surface analysis

Broken surface SEM images of S3 sample are illustrated in Figure 13. The rupture surfaces exhibited brittle fracture. Fractures were caused by carbides, martensite and coarse grains. The rupture line was along the ferrite and martensite boundaries. Chromium element, which looks more intense on the surface than other elements, produced carbide deposits in the structure and caused brittle breakage.

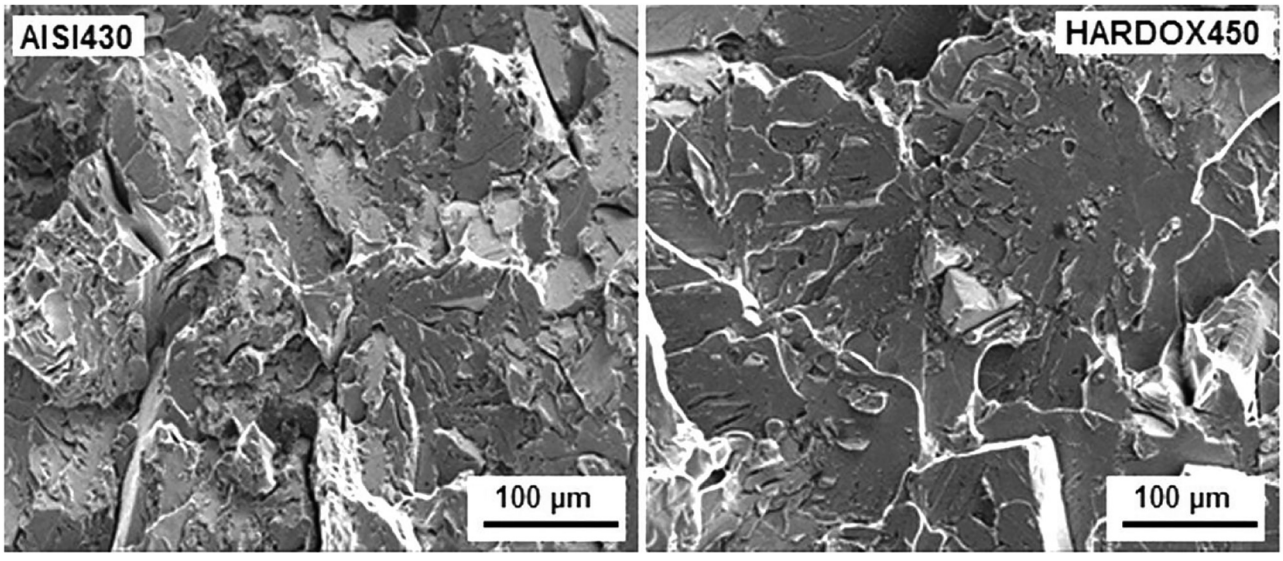

Figure 13: SEM images of the rupture surface of S3 sample.

4 Conclusions

AISI 430 and HARDOX 450 plates were welded with TIG-DSAW. Dissimilar in microstructure and mechanical diffenrences of welded joints were examined. The main conclusions are summarized as follows:

(1) Different AISI 430 and HARDOX 450 steels were successfully joined without chamfering.
(2) Full penetration and hourglass view were obtained with increasing current intensity.
(3) The highest hardness levels were seen as 374 HV for the upper seam and 370 HV for the lower seam. The lowest hardness was determined in the HAZ due to extreme grain size.
(4) The highest tensile strength was 513.59 MPa and the highest impact strength was 77 J.
(5) All of the samples were broken brittle by AISI 430 material. The fracture energy increased with increasing penetration.

Author contributions: All the authors have accepted responsibility for the entire content of this submitted manuscript and approved submission.
Research funding: This work has been supported by Adıyaman University, Scientific Researches Unit (MUFYL/2019-001).
Conflict of interest Statement: No potential conflict of interest was reported by the authors.

References

[1] J. Xiong, S. Liu, and G. Zhang, "Thermal cycle and microstructure of backing weld in double-sided TIG arc horizontal welding of high-strength steel thick plate," *J. Adv. Manuf. Technol.*, vol. 81, pp. 1939–1947, 2010, https://doi.org/10.1007/s00170-015-7248-2.
[2] E. Ahmadi and A. R. Ebrahimi, "Welding of 316L austenitic stainless steel with acti-vated tungsten inert gas process," *J. Mater. Eng. Perform.*, vol. 24, pp. 1065–1071, 2015, https://doi.org/10.1007/s11665-014-1336-6.
[3] A. A. Guimarães and P. R. Mei, "Precipitation of carbides and sigma phase in AISI type 446 stainless steel under working conditions," *J. Mater. Proc. Technol.*, vols. 155–156, pp. 1681–1689, 2004, https://doi.org/10.1016/j.jmatprotec.2004.04.341.
[4] A. K. Lakshminarayanan, K. Shanmugam, and V. Balasubramanian, "Effect of autogenous arc welding processes on tensile and impact properties of ferritic stainless steel joints," *J. Iron Steel Res. Int.*, vol. 16, no. 1, pp. 62–68, 2009, https://doi.org/10.1016/S1006-706X(09)60012-1.
[5] T. Mohandasa, G. M. Reddy, and M. Naveed, "A comparative evaluation of gas tungsten and shielded metal arc welds of a "ferritic" stainless steel," *J. Mater. Proc. Technol.*, vol. 94, nos. 2–3, pp. 133–140, 1999, https://doi.org/10.1016/S0924-0136(99)00092-8.
[6] T. Teker and N. Özdemir, "Weldability and joining characteristic of AISI 430/AISI 1040 steel using keyhole plasma arc welding," *Int. J. Adv. Manuf. Technol.*, vol. 63, pp. 117–128, 2012, https://doi.org/10.1007/s00170-011-3890-5.
[7] K. S. Ramesh, K. S. Akhilendar, S. Sandeep, and P. Aravind, "Investigation on microstructural behavior and mechanical properties of plasma arc welded dissimilar butt joint of austenitic-ferritic stainless steels," *Mater. Today: Proc.*, vol. 5, no. 2, pp. 8008–8015, 2018, https://doi.org/10.1016/j.matpr.2017.11.485.
[8] Y. Xie, Y. Cai, X. Zhang, and Z. Luo, "Characterization of keyhole gas tungsten arc welded AISI 430 steel and joint performance optimization," *J. Adv. Manuf. Technol.*, vol. 99, pp. 347–361, 2018, https://doi.org/10.1007/s00170-018-2257-6.
[9] K. D. Ramkumara, A. Chandrasekhara, A. K. Singha, et al., "Comparative studies on the weldability, microstructure and tensile properties of autogeneous TIG welded AISI 430 ferritic stainless steel with and without flux," *J. Manuf. Proc.*, vol. 20, no. 1, pp. 54–69, 2015, https://doi.org/10.1016/j.jmapro.2015.09.008.
[10] A. G. L. Azevedo, V. A. Ferraresi, and J. P. Farias, "Ferritic stainless steel welding with the A-TIG process," *Weld. Int.*, vol. 24, no. 8, pp. 571–578, 2010, https://doi.org/10.1080/09507110903568794.
[11] T. Teker, "Effect of melt-in and key-hole modes on the structure and mechanical properties of AISI 430 steel welded using plasma transfer arc welding," *Phys. Met. Metallogr.*, vol. 119, no. 7, pp. 669–677, 2018, https://doi.org/10.1134/S0031918X18070116.
[12] Ł. Konat, B. Białobrzeska, and P. Białek, "Effect of welding process on microstructural and mechanical characteristics of HARDOX 600 steel," *Metals*, vol. 7, no. 9, pp. 349–367, 2017, https://doi.org/10.3390/met7090349.
[13] Z. Cheng, J. Huang, Z. Ye, J. Yang, and S. Chen, "Butt brazing of titanium alloys/stainless steel plates by MIG-TIG double-sided arc welding process with copper filler metal," *J. Mater. Res. Technol.*, vol. 8, no. 1, pp. 1566–1570, 2019, https://doi.org/10.1016/j.jmrt.2018.06.009.
[14] ASTM E8M-04, *Standard Test Methods for Tension Testing of Metallic Materials*, West Conshohocken, PA, USA, ASTM International, 2004.
[15] ASTM E23-06, *Standard Test Methods for Notched Bar Impact Testing of Metallic Materials*, West Conshohocken, PA, USA, ASTM International, 2006.
[16] T. Teker, E. M. Karakurt, and F. Demir, "Mechanical property effects of symmetrical hour glass shapes formed during double-sided TIG keyhole arc welding of AISI 1040 joints," *Mater. Test.*, vol. 59, no. 6, pp. 524–529, 2017, https://doi.org/10.3139/120.111041.
[17] J. C. Lippold and D. J. Kotecki, *Welding Metallurgy and Weldability of Stainless Steels*, Hoboken, NJ, USA, John Wiley & Sons, 2005, pp. 88–135.
[18] T. Teker and D. Gençdoğan, "Heat affected zone and weld metal analysis of HARDOX 450 and ferritic stainless steel double sided TIG-joints," *Mater. Test.*, vol. 63, no. 10, pp. 923–928, 2021, https://doi.org/10.1515/mt-2021-0022.

[19] G. Mallaiah, P. R. Reddy, and A. Kumar, "Influence of titanium addition on mechanical properties, residual stresses and corrosion behaviour of AISI 430 grade ferritic stainless steel GTA welds," *Proc. Mater. Sci.*, vol. 6, pp. 1740–1751, 2014, https://doi.org/10.1016/j.mspro.2014.07.204.
[20] P. Sathiya, S. Aravindan, and A. Noorul Haq, "Effect of friction welding parameters on mechanical and metallurgical properties of ferritic stainless steel," *Int. J. Adv. Manuf. Technol.*, vol. 31, pp. 1076–1082, 2007, https://doi.org/10.1007/s00170-005-0285-5.
[21] A. Kumar, G. Sharma, and D. K. Dwivedi, "TIG spot weld bonding of 409 L ferritic stainless steel," *Int. J. Adhes. Adhes.*, vol. 84, pp. 350–359, 2018, https://doi.org/10.1016/j.ijadhadh.2018.04.012.
[22] M. Alizadeh-Sh, S. P. H. Marashi, and M. Pouranvari, "Resistance spot welding of AISI 430 ferritic stainless steel: phase transformations and mechanical properties," *Mater. Des.*, vol. 56, pp. 258–263, 2014, https://doi.org/10.1016/j.matdes.2013.11.022.

The authors of this contribution

Tanju Teker
Prof. Dr. Tanju Teker, born in 1971, works at the University of Sivas Cumhuriyet, Faculty of Technology, Department of Manufacturing Engineering, Sivas, Turkey. He graduated in Metallurgy Education from Gazi University, Ankara, Turkey, in 1997. He received his MSc and PhD degrees from Firat University, Elazig, Turkey, in 2004 and 2010, respectively. He studied metal coating techniques, fusion and solid-state welding methods, casting and wear.

Denizer Gençdoğan
Denizer Gençdoğan, born in 1991, graduated from Metal Teacher, Gazi University, Ankara, Turkey, in 2014. He received his MSc degree from Adıyaman University, Adıyaman, Turkey, in 2020. He is currently studying in Pazarcık Aksu Vocational and Technical Anatolian School, Pazarcık, Kahramanmaraş, Turkey. His research interests fusion welding methods.